Negative Group Delay Theory on Li Topology

Blaise Elysée Guy Ravelo, Lili Wu, Fayu Wan, Wenceslas Rahajandraibe, Nour Murad

IEEE Access
Multidisciplinary | Rapid Review | Open Access Journal

Received February 20, 2020, accepted March 5, 2020, date of publication March 9, 2020, date of current version March 18, 2020.

Digital Object Identifier 10.1109/ACCESS.2020.2979453

Negative Group Delay Theory on Li Topology

BLAISE RAVELO[1], (Member, IEEE), LILI WU[1], FAYU WAN[1], (Member, IEEE), WENCESLAS RAHAJANDRAIBE[2], (Member, IEEE), AND NOUR MOHAMMAD MURAD[3], (Member, IEEE)

[1]School of Electronic and Information Engineering, Nanjing University of Information Science and Technology (NUIST), Nanjing 210044, China
[2]Aix-Marseille University, CNRS, Materials, Microelectronics and Nanoscience Laboratory of Provence (IM2NP) UMR7334, University of Toulon, 83000 Marseille, France
[3]Energy Lab, Institut Universitaire de Technologie at Saint Pierre, 97410 Saint Pierre, France

Corresponding author: Fayu Wan (fayu.wan@nuist.edu.cn)

This work was supported in part by the NSFC under Grant 61971230 and Grant 61601233, in part by the Jiangsu Distinguished Professor program and Six Major Talents Summit of Jiangsu Province under Grant 2019-DZXX-022, in part by the Postgraduate Research and Practice Innovation Program of Jiangsu Province under Grant SJKY19_0974, and in part by the Priority Academic Program Development of Jiangsu Higher Education Institutions (PAPD) Fund.

ABSTRACT This paper investigates an innovative negative group delay (NGD) theory of "li" geometrical shape topology. The li-topology is an outstandingly simple and fully distributed circuit comprised of a coupled line (CL). The li S-parameter model taking into account the CL coupling coefficient, delay and attenuation is established. The NGD analysis showing the possibility to generate NGD condition with respect to the li topology parameters is developed. The NGD characteristics as NGD value, center frequency, bandwidth, transmission and reflection coefficient are expressed. The li-NGD theory is validated with two proofs-of-concept implemented in microstrip technology. Calculated models, simulations and measurements are in good correlation. As expected, bandpass NGD presenting center frequency at approximately 2.56 GHz and 0.92 GHz with NGD level of approximately −0.9 ns and −3.7 ns were realized with the small and large li prototypes. Outstanding time-domain analyses explaining the bandpass NGD meaning, with innovatively low attenuation output, were also presented. The time-domain results highlight li-output pulse signal envelopes in time advance without violating the causality.

INDEX TERMS Distributed circuit, li-topology, microwave theory, negative group delay (NGD), S-matrix modelling.

I. INTRODUCTION

The intriguing abnormal media with counterintuitive negative refractive index (NRI) were theoretically studied by Brillouin in 1960s [1]. This theoretical investigation was initially focused on the anomalous dispersive and absorptive optical media in the frequency domain [1], [2]. It was shown that the negative group delay (NGD) phenomenon can be occurred around the resonance frequency of the absorptive media.

The interpretation of the NRI phenomenon was made with the link between the group velocity. Indeed, this later one is implicitly negative when the refractive index is negative. More understandable investigation about this abnormal phenomenon was suggested in 1970 [2] using time-domain analysis. Analytical study of Gaussian light pulse propagating through an anomalous dispersion medium was proposed. The practical confirmations of the abnormal NRI were performed with the first experimentation of NGD in 1980s [4], [5]. Some decades later, the NGD phenomenon was verified in the optical wavelengths to introduce NRI transmission line (TL) [5]. This counterintuitive NRI aspect was also approved with NGD observations in a photonic crystal structure [6]. Knowing the existence of the NGD phenomenon in the optical wavelengths, the question about its existence in the microwave range attracted the attention of microwave design engineer researchers.

The first verification of NGD phenomenon with microwave circuit was performed in 1990s [7], [8]. In 2000s, NGD passive circuits built with R, L and C lumped elements inspired from periodical NRI TLs in parallel with the deployment of metamaterial concept were designed and tested [9]–[11]. At that period, the NGD circuit design was particularly complex. Therefore, curious questions have been asked on the NGD meaning and the understanding of its physical interpretation. Theoretical approaches based on elementary circuits are necessary for the further microwave

The associate editor coordinating the review of this manuscript and approving it for publication was Wenjie Feng.

circuit knowledge about the NGD function. The confirmation of NGD function existence with lumped circuits opens the possibility for RF and microwave engineers to design simpler NGD topologies. Theoretical investigations [9]–[18] were also realized, for example, with two-port circuits defined by the S-matrix:

$$[S(j\omega)] = \begin{bmatrix} S_{11}(j\omega) & S_{12}(j\omega) \\ S_{21}(j\omega) & S_{22}(j\omega) \end{bmatrix} \quad (1)$$

by means of the group delay (GD) definition:

$$\tau(\omega) = -\frac{\partial\varphi(\omega)}{\partial\omega} \quad (2)$$

from the transmission parameter phase:

$$\varphi(\omega) = \angle S_{21}(j\omega) \quad (3)$$

with ω is the angular frequency variable. Therefore, theoretical synthesis methods of lumped components based NGD circuits were developed [12], [13]. The NGD concept understanding lead to tentative NGD application propositions [14]–[23] notably in the field of RF and microwave engineering. A microwave group delay (GD) time adjuster was proposed in [14], [15]. A GD equalized ultra-wide band amplifier using NGD circuits was introduced in [16]. A design method of feedforward amplifier for the bandwidth enhancement was presented in [17]. The NGD function was also used to realize a bilateral gain-compensated circuit [18]. By cascading with a TL, the NGD function enabled to synthesize a frequency independent phase shifter [19]. The NGD circuits were implemented to realize non-Foster reactive elements [20], [21] which are used to design an arbitrary-angle squint-free beamforming in series-fed antenna arrays [22]. The NGD function was more recently used to design a tunable delay shifter [23]. A bi-directional amplifier using NGD matched circuits was designed [24]. Despite this progressive development of NGD applications, further efforts have to be conducted to overcome the limitations in terms of losses [9]–[11], operation frequency bandwidth, design complexity and the implicit asymptotic limits of active circuits [25].

To overcome these limitations, research works have been made to develop design method of different topologies of distributed NGD networks [26]–[29]. One of the simplest distributed NGD circuits is based on the use of two parallel lines [26]–[29]. A design method of NGD microwave circuits based on signal interference technique was introduced in [26]. An analysis of three parallel lines NGD structure was proposed in [27]. A transmission type NGD structure was developed in [28]. A feedback delayed coupler based coupled lines (CLs) was introduced in [29]. But all these NGD circuits operate with rather complex topology. It is particularly important, for all RF and microwave research community to investigate on simpler NGD circuits with well-known topologies. This curiosity constitutes a best way to make the NGD function to be familiar and to be understandable to all RF and microwave design engineers who are mostly do not understand the existence of NGD function.

For this reason, this paper focused on *a completely innovative NGD theory applied to the simplest elementary CL topology is intuitively presented. This original idea, which was never be studied before, is deepened by investigating the distributed structure having a simple "li"-shape geometry. In difference to the published research works based on the CL structure, the li-NGD new theory elaborate the GD detailed expression by taking into account the inherent imperfections of CL as the propagation delay and transmission coefficient.*

The present paper is organized in five main sections:

- Section II is focused on the general S-matrix modelling of two-port li-topology. The analytical model will be elaborated from the topological equivalent diagram.
- Section III is the analytical development of the NGD theory. After the GD expression, the NGD analysis is established. The GDs at particular frequencies are formulated and analyzed. The NGD properties and characteristics as functions of the li-topology parameters will be expressed.
- Hence, Section IV will explore the li-NGD theory validation results. After the proof-of-concept (POC) description, the simulated and experimented results will be discussed. Comparisons between simulated and measured GDs will be performed.
- Comparison of NGD performances are discussed in Section V.
- Lastly, Section VI is the conclusion of the paper.

II. S-MATRIX MODEL OF THE PROPOSED CL-BASED LI-SHAPE TOPOLOGY

Acting as a microwave circuit, the elaboration of the NGD theory must be preceded by S-matrix modelling. After the structural description, the following subsections introduces the methodology of the li S-matrix modelling.

A. DESCRIPTION OF THE LI SHAPE STRUCTURE UNDER STUDY

Fig. 1(a) depicts the structural geometry of the li circuit. This distributed circuit is a two-port topology composed of parallel CL($\zeta, R_0, a, \tau_1, \tau_2$). This CL is defined by its coupling coefficient ζ and characteristic impedance R_0. The li topology equivalent diagram is depicted in Fig. 1(b).

Different to the NGD work performed before [28]–[30], the present study is dealing with the CL imperfection represented by the coupled way delay τ_1, and the direct way attenuation a and delay τ_2. This imperfection may be roughly explored in certain microwave engineering literature but none of them investigates about the NGD function as we did in the present paper.

B. S-MATRIX MODELLING METHODOLOGY

After brief recall on the CL S-matrix, the modelling methodology of the li-topology will be developed in the next paragraphs.

1) CL S-Matrix

The CL constituting the fully distributed li-topology is a four-port system referenced with internal port numbers ❶, ❷,

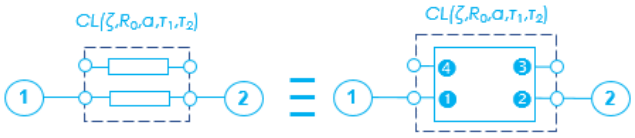

FIGURE 1. (a) Configuration of "li" topology under study and (b) its equivalent diagram.

❸ and ❹ as depicted in Fig. 1(b). The S-parameter model of this CL including the inherent imperfections as propagation delay and transmission coefficient can be written as:

$$[S_{CL}] = \begin{bmatrix} 0 & \varpi & 0 & e^{-j\omega\tau_1}\zeta \\ \varpi & 0 & e^{-j\omega\tau_1}\zeta & 0 \\ 0 & e^{-j\omega\tau_1}\zeta & 0 & \varpi \\ e^{-j\omega\tau_1}\zeta & 0 & \varpi & 0 \end{bmatrix}, \quad (4)$$

by denoting the angular frequency variable ω and the complex number $j = \sqrt{-1}$ with:

$$\begin{cases} \zeta_0 = \sqrt{1-\zeta^2} \\ \varpi = -ja\, e^{-j\omega\tau_2}\zeta_0. \end{cases} \quad (5)$$

2) LI-TOPOLOGY S-MATRIX MODEL

The S-matrix modelling of the li-topology depends systematically to the reduction of CL one introduced previously in (4). The analytical approach to determine this S-matrix can traditionally be elaborated from the consideration of CL input and output wave powers a_m and b_m ($m = \{1, 2, 3, 4\}$). In fact, we can recall the analytical matrix relationship between [S_{CL}] and the CL access port wave powers:

$$\begin{bmatrix} b_1 \\ b_2 \\ b_3 \\ b_4 \end{bmatrix} = [S_{CL}] \times \begin{bmatrix} a_1 \\ a_2 \\ a_3 \\ a_4 \end{bmatrix}. \quad (6)$$

As ports ❸ and ❹ are open-ended, the associated reflection coefficient should be equal to 1. Therefore, the $[S_{CL}]$ matrix reduction can be realized knowing this reflection coefficient:

$$\begin{cases} b_3 = a_3 \\ b_4 = a_4. \end{cases} \quad (7)$$

C. S-MATRIX REDUCTION APPROACH

Assumed as a two-port symmetric and passive topology, the frequency-dependent S-matrix of the li-topology can be merely written as:

$$[S(j\omega)] = \begin{bmatrix} S_{11}(j\omega) & S_{21}(j\omega) \\ S_{21}(j\omega) & S_{11}(j\omega) \end{bmatrix}. \quad (8)$$

Following the configuration of the circuit proposed in Fig. 1(a), S_{11} and S_{21} can be analytically determined by the reduction of matrix (4). Substituting (7) into (6), we have the reduced quantities:

$$\begin{bmatrix} a_3 \\ a_4 \end{bmatrix} = \begin{bmatrix} S_{CL_{31}} & S_{CL_{32}} \\ S_{CL_{41}} & S_{CL_{42}} \end{bmatrix} \times \begin{bmatrix} a_1 \\ a_2 \end{bmatrix} + \begin{bmatrix} S_{CL_{33}} & S_{CL_{34}} \\ S_{CL_{43}} & S_{CL_{44}} \end{bmatrix} \times \begin{bmatrix} a_3 \\ a_4 \end{bmatrix}. \quad (9)$$

The algebraic solutions yielding from this matrix equation can be expressed as:

$$\begin{bmatrix} a_3 \\ a_4 \end{bmatrix} = \begin{bmatrix} 1 - S_{CL_{33}} & -S_{CL_{34}} \\ -S_{CL_{43}} & 1 - S_{CL_{44}} \end{bmatrix}^{-1} \begin{bmatrix} S_{CL_{31}} & S_{CL_{32}} \\ S_{CL_{41}} & S_{CL_{42}} \end{bmatrix} \times \begin{bmatrix} a_1 \\ a_2 \end{bmatrix}. \quad (10)$$

The simplification of this matrix expression gives the following relationship:

$$\begin{bmatrix} a_3 \\ a_4 \end{bmatrix} = \frac{1}{\upsilon} \begin{bmatrix} S_{CL_{31}}(1 - S_{CL_{44}}) + S_{CL_{34}}S_{CL_{41}} & S_{CL_{32}}(1 - S_{CL_{44}}) + S_{CL_{34}}S_{CL_{42}} \\ S_{CL_{41}}(1 - S_{CL_{33}}) + S_{CL_{31}}S_{CL_{43}} & S_{CL_{42}}(1 - S_{CL_{33}}) + S_{CL_{32}}S_{CL_{43}} \end{bmatrix} \times \begin{bmatrix} a_1 \\ a_2 \end{bmatrix} \quad (11)$$

where the divider term is:

$$\upsilon = 1 + S_{CL_{33}}(S_{CL_{44}} - 1) - S_{CL_{44}} - S_{CL_{34}}S_{CL_{43}}. \quad (12)$$

The li-topology S-parameter model can be constructed from the complementary part of (9). Substituting this quantity into the first and second line of linear equation from (6), the previous relationship can be rewritten as:

$$\begin{bmatrix} b_1 \\ b_2 \end{bmatrix} = \begin{bmatrix} S_{CL_{11}} & S_{CL_{12}} \\ S_{CL_{21}} & S_{CL_{22}} \end{bmatrix} \times \begin{bmatrix} a_1 \\ a_2 \end{bmatrix} + \begin{bmatrix} S_{CL_{13}} & S_{CL_{14}} \\ S_{CL_{23}} & S_{CL_{24}} \end{bmatrix} \times \begin{bmatrix} a_3 \\ a_4 \end{bmatrix}. \quad (13)$$

After detailed analytical calculation, we get the associated S-matrix which will be theoretically explored in the next subsection.

D. FREQUENCY-DEPENDENT PARAMETERS ANALYSIS

The frequency-dependent expression of the li-topology S-matrix elements was established from the operation of relations (11) and (12). It can be derived from the analytical operation that the li-topology reflection and transmission coefficients are written as respectively:

$$S_{11}(j\omega) = \frac{e^{-2j\omega\tau_1}\zeta^2}{1 + a^2e^{-2j\omega\tau_2}\zeta_0^2} \quad (14)$$

$$S_{21}(j\omega) = \frac{ja\, e^{-j\omega\tau_2}\zeta_0\left[a^2e^{-2j\omega\tau_2}(e^{-2j\omega\tau_1}\zeta^2 - 1) - 1 - \zeta^2\right]}{1 + a^2e^{-2j\omega\tau_2}\zeta_0^2}. \quad (15)$$

Acting as a fully distributed topology, the S-parameters are periodic expressions with period:

$$\omega_p = 2\pi f_p = \frac{2\pi}{m_1\tau_1} = \frac{2\pi}{m_2\tau_2}. \quad (16)$$

If there are integers whose smallest verify the relationship:

$$\frac{m_1}{m_2} = \frac{\tau_1}{\tau_2}. \quad (17)$$

The associated magnitudes are given by:

$$S_{11}(\omega) = |S_{11}(j\omega)| = \frac{\zeta^2}{\sqrt{1 + a^4\zeta_0^4 + 2a^2\zeta_0^2\cos(2\omega\tau_2)}} \quad (18)$$

$$S_{21}(\omega) = |S_{21}(j\omega)| = \frac{a\,\zeta_0^2 \sqrt{\begin{array}{l} 2a^2(1-\zeta^4)\cos(2\omega\tau_2)+ \\ (1+a^4)(1+\zeta^4)+2a^2\zeta^2 \\ \zeta_0^2\cos\left[2\omega(\tau_2-\tau_1)\right] \end{array}}}{\sqrt{1+a^4\zeta_0^4+2a^2\zeta_0^2\cos(2\omega\tau_2)}}. \tag{19}$$

The corresponding transmission phase is expressed as:

$$\varphi(\omega) = \varphi_a(\omega) - \varphi_b(\omega) \tag{20}$$

with:

$$\varphi_a(\omega) = \frac{\pi}{2} - \arctan\left\{\frac{\zeta^2\cos\left[\omega(\tau_2-2\tau_1)\right]+(1+a^2\zeta_0^2)\cos(\omega\tau_2)}{\zeta^2\sin\left[\omega(\tau_2-2\tau_1)\right]+(1-a^2\zeta_0^2)\sin(\omega\tau_2)}\right\} \tag{21}$$

$$\varphi_b(\omega) = \arctan\left[\frac{\sin(2\omega\tau_2)}{a^2\zeta_0^2+\cos(2\omega\tau_2)}\right]. \tag{22}$$

III. LI-TOPOLOGY NGD ANALYSIS

The present section is dedicated to the li topology NGD theory. The GD is calculated from the transmission coefficient. Then, NGD analysis is elaborated as a function of the li topology parameters.

A. FREQUENCY-DEPENDENT GD EXPRESSION

By definition, the li topology GD is calculated from equation (2). By means of the transmission phase given in (20), we have the GD written as:

$$\tau(\omega) = \tau_b(\omega) - \tau_a(\omega) \tag{23}$$

with:

$$\begin{cases} \tau_a(\omega) = -\dfrac{\partial\varphi_a(\omega)}{\partial\omega} \\ \tau_b(\omega) = -\dfrac{\partial\varphi_b(\omega)}{\partial\omega}. \end{cases} \tag{24}$$

By taking into account the phase angle introduced in (21), we have:

$$\tau_a(\omega) = \frac{a_0+a_1\cos(2\omega\tau_1)+a_2\cos\left[2\omega(\tau_2-\tau_1)\right]}{\begin{array}{l} b_0+b_1\cos(2\omega\tau_1)+b_2\cos(2\omega\tau_2) \\ +b_3\cos\left[2\omega(\tau_2-\tau_1)\right] \end{array}} \tag{25}$$

with:

$$\begin{cases} a_0 = (1+\zeta^4-a^4\zeta_0^4)\tau_2 - 2\zeta^4\tau_1 \\ a_1 = 2\zeta^2(\tau_2-\tau_1) \\ a_2 = -2a^2\zeta^2\zeta_0^2\tau_1 \\ b_0 = 1+\zeta^4+a^4\zeta_0^4 \\ b_1 = 2\zeta^2 \\ b_2 = 2a^2\zeta_0^2 \\ b_3 = 2a^2\zeta^2\zeta_0^2. \end{cases} \tag{26}$$

The derivation of the phase angle expressed previously in (22) with respect to ω gives:

$$\tau_b(\omega) = \frac{2\tau_2\left[1+a^2\zeta_0^2\cos(2\omega\tau_2)\right]}{1+a^4\zeta_0^4+2a^2\zeta_0^2\cos(2\omega\tau_2)}. \tag{27}$$

This equation explains that the li GD depends linearly on the CL delays τ_1 and τ_2.

B. NGD PROPERTIES

The analytical properties related to the li topology are examined in the present subsection.

1) NGD EXISTENCE CONDITION

The NGD analysis consists theoretically in characterizing the NGD bandpass behavior of the li topology with the functions GD and S_{21}. Basically, the NGD analysis leads also to determine the NGD existence by verifying the following condition:

$$\tau(\omega) < 0. \tag{28}$$

Around the NGD center frequency where:

$$\tau_o = \tau(\omega=\omega_o) = \tau_{\min} < 0 \tag{29}$$

the NGD cut-off frequencies ω_1 and $\omega_2 > \omega_1$ are defined as the roof of equation:

$$\tau(\omega) = 0. \tag{30}$$

The NGD bandwidth is defined by:

$$\Delta\omega = \omega_2 - \omega_1. \tag{31}$$

2) BEHAVIORAL ANALYSIS AT LOW FREQUENCIES

Before the deep analysis, we can verify intuitively that at very low frequencies $\omega \approx 0$, we have:

$$S_{11}(\omega\approx 0) = \frac{\zeta^2}{1+2a^2\zeta_0^2} \tag{32}$$

$$S_{21}(\omega\approx 0) = \frac{a\,\zeta_0^2\sqrt{\begin{array}{l} 2a^2(1+\zeta^2-\zeta^4)+ \\ (1+a^4)(1+\zeta^4)+\zeta_0^2 \end{array}}}{1+a^2\zeta_0^2}. \tag{33}$$

Thus, the GD expressed in (23) is simplified as:

$$\tau(\omega\approx 0) = \frac{\begin{array}{l} 2\zeta^2(1+a^2\zeta_0^2)\tau_1+ \\ \left[1+\zeta^2+a^2(2-3\zeta^2+\zeta^4)+a^4\zeta_0^4\right]\tau_2 \end{array}}{(1+a^2\zeta_0^2)(1+\zeta^2+a^2\zeta_0^2)}. \tag{34}$$

This GD is unconditionally positive. Consequently, the li-topology cannot behave as a low-pass NGD function.

C. NGD PERFORMANCE

The NGD performance depends on the NGD bandwidth and also the S-parameter values as insertion and reflection coefficient around the center frequency.

1) NGD SPECIFIC FREQUENCIES

Acting as linear passive circuit, the spectrum of GD and the transmission coefficient magnitude $|S_{21}(j\omega)|$ or:

$$|S_{21}(j\omega)|^2 = \frac{a^2\,\zeta_0^4\left\{\begin{array}{l} 2a^2(1-\zeta^4)\cos(2\omega\tau_2)+ \\ (1+a^4)(1+\zeta^4)+2a^2\zeta^2 \\ \zeta_0^2\cos\left[2\omega(\tau_2-\tau_1)\right] \end{array}\right\}}{1+a^4\zeta_0^4+2a^2\zeta_0^2\cos(2\omega\tau_2)} \tag{35}$$

must present a similar behavior. Meanwhile, the two quantities must present the same optimal angular frequencies $\omega = \omega_o$:

$$S_{21}^2(\omega = \omega_o) = S_{21_{\min}}^2. \tag{36}$$

When the transmission coefficient reaches its minimal value, the reflection coefficient must complementarily reach its maximum:

$$S_{11}^2(\omega = \omega_o) = S_{11_{\max}}^2. \tag{37}$$

Therefore, inversely, the denominator must be minimal:

$$S_{11_{\max}}^2 \Rightarrow \left|1 + a^4\zeta_0^4 + 2a^2\zeta_0^2\cos(2\omega\tau_2)\right|_{\min}. \tag{38}$$

It yields as the terms:

$$1 + a^4\zeta_0^4 \tag{39}$$

and:

$$2a^2\zeta_0^2 \tag{40}$$

are positive, for the integer $m = \{1, 2, \ldots\}$, the optimal angular frequency from expression (18) when:

$$\cos(2\omega_o\tau_2) = -1 \Rightarrow \omega_o(m) = \frac{(2m+1)\pi}{2\tau_2}. \tag{41}$$

In this case, the reflection and transmission coefficients introduced in (18) and (19) become respectively:

$$S_{11}(\omega_o) = \frac{\zeta^2}{1 - a^2\zeta_0^2} \tag{42}$$

$$S_{21}(\omega_o) = \frac{a\,\zeta_0^2\sqrt{\begin{matrix}(1+a^4)(1+\zeta^4) + 2a^2\zeta^2 \\ -2a^2(1-\zeta^4) + \zeta_0^2\cos\left(\frac{\pi\tau_1}{\tau_2}\right)\end{matrix}}}{1 - a^2\zeta_0^2}. \tag{43}$$

For the better evidence of existing NGD aspect, let us consider the particular case where:

$$\tau_1 = \frac{\tau_2}{2}. \tag{44}$$

Thus, the GD expressed in (22) is simplified as:

$$\frac{\tau(\omega_o)}{\tau_2} = \frac{1 - 2\zeta^2 + 2a^2\zeta_0^2 + a^4(1-\zeta^2)^2}{(1+a^2)(1-\zeta^2)\left[1 + a^2(1-\zeta^2)\right]}. \tag{45}$$

This expression is negative when:

$$\zeta \geq \zeta_{\min} = \sqrt{1 + \frac{1 + a^2 - \sqrt{1 + 2a^2 + 2a^4}}{a^4}}. \tag{46}$$

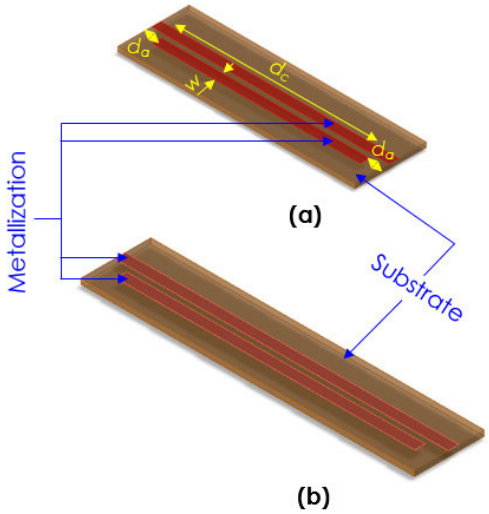

FIGURE 2. 3D design of (a) S- and (b) L-li circuit POCs.

2) NGD FOM

The NGD topology performance depends mainly on:

- the NGD bandwidth $\Delta\omega$;
- the GD $\tau_o = \tau(\omega_o)$ at the NGD center frequency ω_n,

and secondarily to:

- the transmission coefficient $S_{21}(\omega_o)$;
- the reflection coefficient $S_{11}(\omega_o)$.

Accordingly, the NGD performance can be more generally reformulated with the following equation:

$$FoM_{NGD} = \Delta\omega \cdot \tau(\omega_o) \cdot \sqrt{\frac{S_{21}(\omega_o)}{S_{11}(\omega_o)}}. \tag{47}$$

To verify the relevance of the established li NGD theory, simulation and experimental results are discussed in the next section.

IV. SIMULATIONS AND EXPERIMENTAL VALIDATIONS OF THE LI NGD TOPOLOGY

As POC, two microstrip li prototypes have been designed, simulated, fabricated and tested. The simulations are carried out with the EM tool ADS®Momentum from Keysight Technologies®. After the li-NGD POC description, the computed, simulated and experimental results will be compared in the next subsections.

A. SINGLE DESCRIPTION OF LI NGD POC

The li NGD prototypes were designed after optimization of physical lengths and space of the parallel TLs. Fig. 2(a) and Fig. 2(b) display the 3D design of the small (“S”) and large (“L”) li prototypes implemented in microstrip technology. These prototypes are designed as fully distributed circuits. The photographs of the fabricated corresponding circuit are presented in Figs. 3. The parameters of the substrate, metallization, and S- and L-li prototypes are addressed in Table 1.

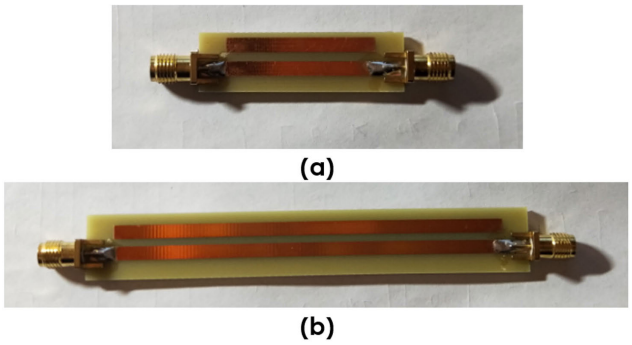

FIGURE 3. Photographs of (a) S- and (b) L-li circuit POCs.

TABLE 1. Fabricated li prototypes' parameters.

Components		*Description*	*Parameter*	*Value*
Dielectric substrate		Material	FR4-epoxy	-
		Relative permittivity	ε_r	5
		Loss tangent	$\tan(\delta)$	0.02
		Thickness	h	1.6 mm
Metallization		Material	Copper (Cu)	-
		Thickness	t	35 µm
		Conductivity	σ	58 MS/m
Coupled CL	"S"-li	Width	w	3 mm
		Length	d_c	30 mm
		Interspace	s	1.8 mm
		Coupling coefficient	ζ	-19 dB
		Attenuation	a	-0.3 dB
		Characteristic impedance	Z_c	47 Ω
		Coupled way delay	τ_1	0.07 ns
		Direct way delay	τ_2	0.3 ns
	"L"-li	Width	w	3 mm
		Length	d_c	85 mm
		Interspace	s	1.6 mm
		Coupling coefficient	ζ	-18 dB
		Attenuation	a	-0.25 dB
		Characteristic impedance	Z_c	46 Ω
		Coupled way delay	τ_1	0.2 ns
		Direct way delay	τ_2	0.82 ns
Access lines		Width	w	3 mm
		Physical length	d_a	5 mm

B. PARAMETRIC ANALYSIS

To get an overview about the CL coupling coefficient and physical influences on the NGD function, parametric analyses will be discussed in the two following paragraphs. The developed analyses were carried out by varying the space s and the physical length d_c of li circuit. This preliminary numerical study is realized with ADS®simulator from Keysight Technologies®.

1) INFLUENCE OF CL COUPLING COEFFICIENT

The CL delay was controlled by changing the two parallel line physical space s from 1 mm to 2 mm. During the present analysis, d_c was kept equal to 70 mm. The S-parameter parametric simulations have been performed from 0.8 GHz to 1.63 GHz. Figs. 4 display the cartographies of results showing the GD, transmission and reflection coefficients versus frequency and s.

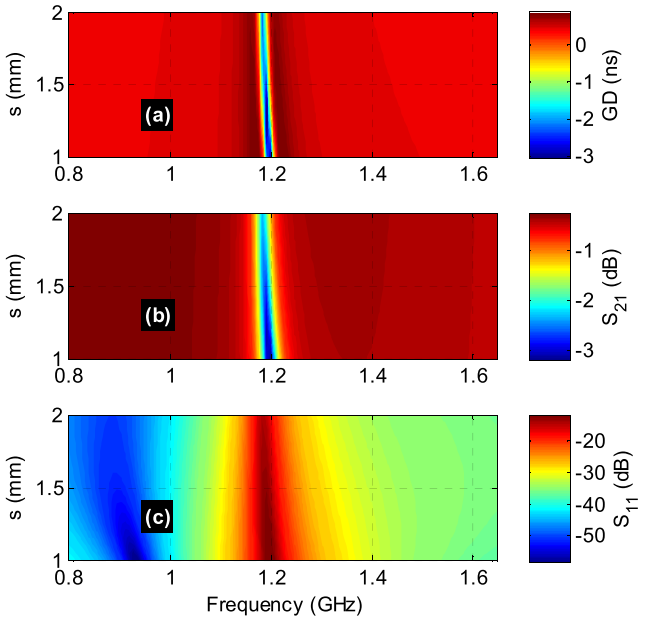

FIGURE 4. (a) GD, (b) S_{21} and (b) S_{11} of li circuit versus physical space s and frequency.

We understand from Fig. 4(a) that the NGD absolute value increases with the coupling coefficient. The influence to the NGD center and bandwidth is insignificant. As illustrated in Fig. 4(b) and in Fig. 4(c), the transmission coefficient remains lower than 3 dB and the reflection coefficient is higher than 10 dB in the whole range of the frequency and also of physical space s.

2) INFLUENCE OF CL DELAY

The CL delay was controlled by changing the physical length d_c. from 20 mm to 100 mm. During the present analysis, s was kept equal to 1.8 mm. Figs. 5 display the cartographies of parametric simulated results versus frequency and d_c.

Fig. 5(a) explains that the GD center frequency varies inversely to d_c or much more generally to the CL delay. However, the NGD absolute value and bandwidth are insensitive to the CL delay. Fig. 5(b) illustrates that the transmission coefficient behaves similarly to the GD with very low attenuation less than 3 dB in the considered range of simulation parameters. As shown in Fig. 5(c), the reflection coefficient is better than 10 dB.

C. DISCUSSION ON EXPERIMENTAL RESULTS

The present subsection presents the experimental validation results of the previously described S- and L-li fabricated prototypes introduced in Figs. 2 and Figs. 3.

1) EXPERIMENTAL SETUP

Fig. 6 presents the configuration of the experimental setup by using a two-port Vector Network Analyzer (VNA). The S-parameter measurements are completed using the VNA from Rohde&Schwarz®referenced ZNB 20 and specified

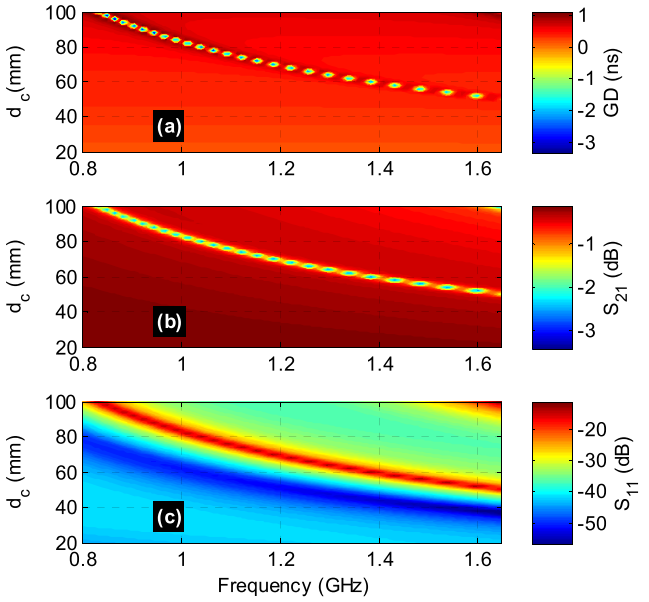

FIGURE 5. (a) GD, (b) S_{21} and (b) S_{11} of li circuit versus physical length d_c and frequency.

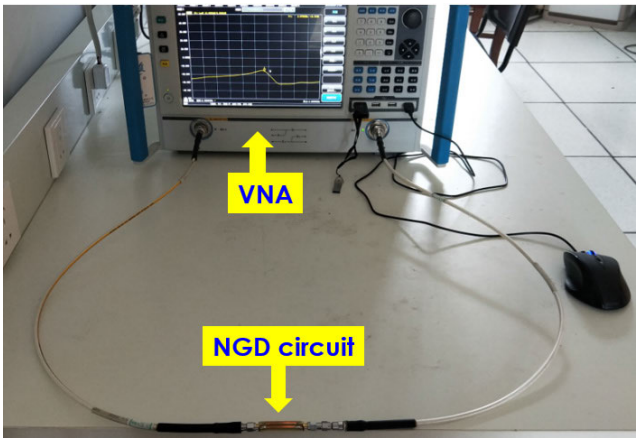

FIGURE 6. Configuration of li-prototype experimental setup.

by frequency band 100 kHz to 20 GHz. The S-parameter measurement was performed under the SOLT calibration by using the kit 85052D from Keysight Technologies®.

2) VALIDATION RESULTS WITH S-LI POC

The comparisons between calculated (dotted "Model" line), simulated (solid "ADS" line) and measured (dashed "Meas." line) results from the S-li prototype shown in Fig. 2(a) and in Fig. 2(b) are introduced in Figs. 7. The results plotted between 2.4 GHz and 2.7 GHz are rather in good correlation and highlights the feasibility of bandpass NGD function with the S-li topology. The NGD circuit specific characteristics are indicated in Table 2. The slight differences between the calculated, simulated and measured S-parameters, NGD central frequency shift are mainly due to classical fabrication realistic effects, substrate parameter inaccuracies and numerical computation inaccuracies from Momentum®. As expected, the feasibility to generate bandpass NGD function is confirmed by the GD plotted in Fig. 7(a) with center frequency

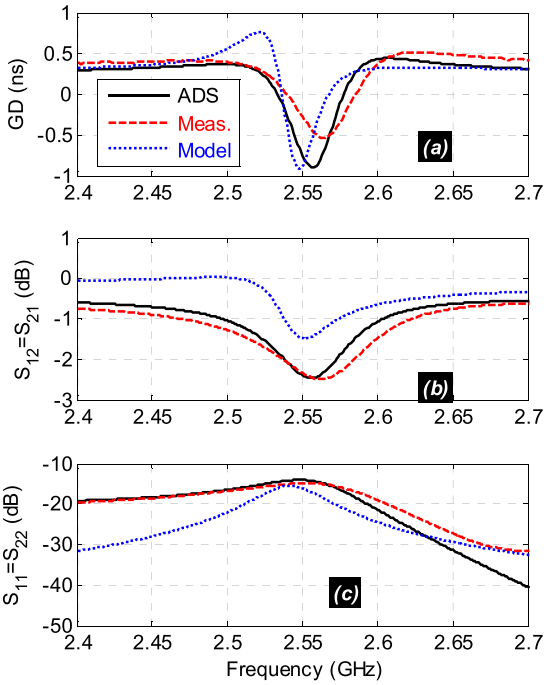

FIGURE 7. Comparisons of measured and simulated (a) GD, (b) transmission and (c) reflection parameters from the S-li prototype shown in Fig. 2(a) and Fig. 3(a).

TABLE 2. S-li circuit NGD specifications.

Validation Method	f_o (GHz)	$\tau(f_o)$ (ns)	*BW* (MHz)	$S_{21}(f_o)$ (dB)	$S_{11}(f_o) \approx S_{22}(f_o)$ (dB)
Simu.	2.557	-0.89	45	-2.46	-14.05
Meas.	2.564	-0.54	46	-2.49	-14.86
Model	2.547	-0.91	31	-1.5	-15.51

f_o around 2.555 GHz indicated in Table 2. The NGD value is slightly higher than −1 ns over the NGD bandwidth of about 45 MHz.

In addition to the NGD aspect, as shown in Fig. 7(b), the S-li prototype generates a particularly interesting transmission coefficient better than 2.5 dB. As seen in Fig. 7(c), it presents also a reflection coefficient better than 14 dB in the NGD bandwidth.

3) VALIDATION RESULTS WITH l-LI POC

Figs. 8 display the comparisons between the calculated, simulated and measured results from the L-li prototype shown in Fig. 2(b) and Fig. 3(b). These validation results are plotted between 0.89 GHz and 0.96 GHz. The center frequency is widely lower than the S-li one because the L-li circuit has larger CL physical length. Despite the differences between the plots of S-parameter responses, we can emphasize that the simulated and measured results validate the behaviors of the ideally calculated ones.

The discrepancies between the different results are generally due to the same reason as pointed in the previous paragraph of S-li prototype.

The main differences between the calculated and simulated/measured reflection coefficients are caused by:

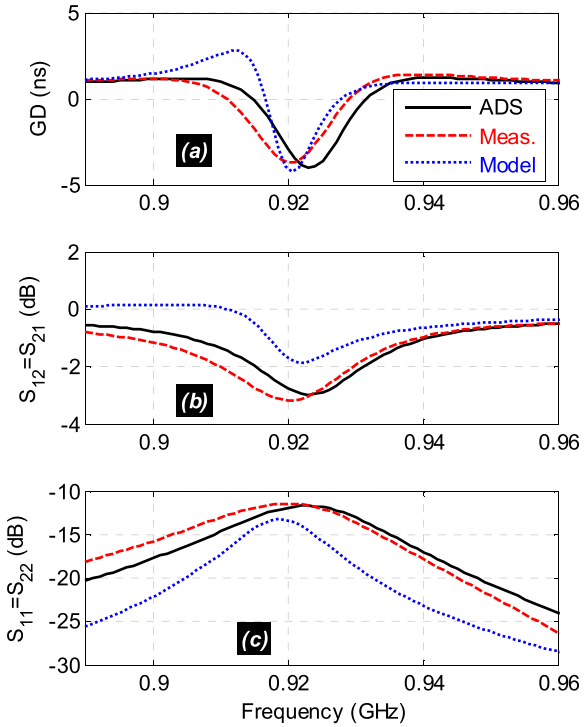

FIGURE 8. Comparisons of measured and simulated (a) GD, (b) transmission and (c) reflection parameters from the L-li prototype shown in Fig. 2(b) and Fig. 3(b).

TABLE 3. L-li circuit NGD specifications.

Validation Method	f_o (GHz)	$\tau(f_o)$ (ns)	BW (MHz)	$S_{21}(f_o)$ (dB)	$S_{11}(f_o) \approx S_{22}(f_o)$ (dB)
Simu.	0.923	-4.03	17	-2.97	-11.68
Meas.	0.92	-3.72	18	-3.18	-11.43
Model	0.9205	-4.29	11	-1.85	-13.21

- Unintentional parasitic effects of the connectors soldering which induces further unmatching effects visibly occurred on the input reflection parameters,
- and 3D structure electromagnetic behavior of CL constituting the li circuit which is not perfectly ideal as considered in the analytical calculation.

The associated NGD circuit characteristics are summarized in Table 3. The model, simulation and measurements are rather in good correlation and confirm the bandpass NGD function feasibility of li topology. As indicated in Table 3, in this case, the NGD value is of about -3.7 ns at the NGD center frequency around 0.92 GHz. For this L-li prototype, the NGD absolute value is much higher but the NGD bandwidth is narrower and it is approximately equal to 18 MHz.

In the NGD L-li bandwidth, the maximal attenuation loss from measurement is of about 3.18 dB. The input and output reflection coefficient are better than 11 dB.

D. TIME-DOMAIN ANALYSES

The significance of bandpass NGD function is illustrated in this subsection with time-domain analyses which are carried out. The numerical computations were made via convolution between the measured S-parameter touchstone model and gaussian modulating since carrier signal with frequency equal to the NGD center frequencies. Few published papers present time domain results a bandpass NGD passive circuit in the microwave frequency with less output attenuation as obtained herein with li circuits.

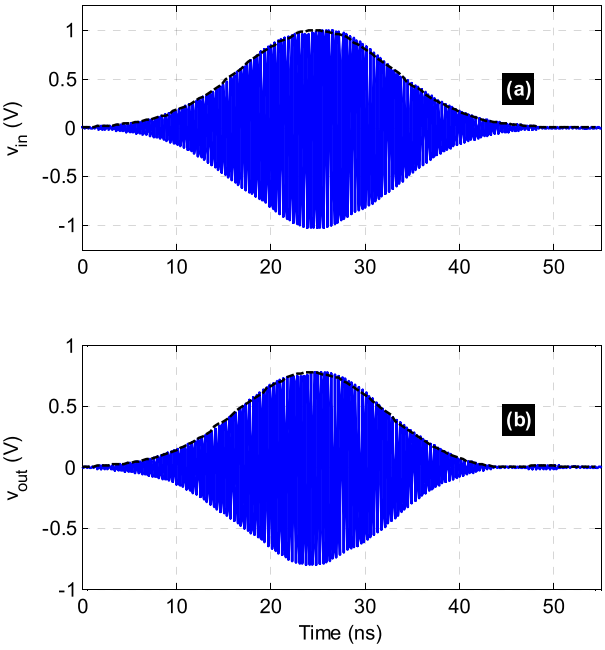

FIGURE 9. Input (in top) and output (in bottom) transient signals from S-li NGD circuit.

1) S-LI TIME-DOMAIN RESPONSE

To perform the time-domain analysis of the S-li prototype, we considered an input pulse signal with spectrum belonging in the NGD bandwidth of the GD plotted earlier in Fig. 7(a). The considered input is an analytical signal plotted in top of Figs. 9. This input signal presented in Fig. 9(a) presents a gaussian waveform defined with time-width of about 50 ns with 1 V amplitude modulating a sine carrier $f_o = 2.564$ GHz. The S-li NGD circuit output is plotted in bottom of Fig. 9(b).

To highlight the NGD function effect from the S-li circuit, the input (black solid line) and output (red dashed line) signal envelopes are plotted in Figs. 10. These input and output signals are notably well-correlated. As predicted by the transmission coefficient plotted earlier in Fig. 7(b), the output is slightly attenuated compared to the input. The normalized signals displayed in Fig. 10(b) demonstrates the capacity of the S-li circuit to generate an output envelope in time advance compared to its input without violating the causality. The output time-advance of leading and trailing edges can be understood more with zoom in plot of Fig. 10(c) and Fig. 10(d), respectively. The trailing edge shows more significant advance because of the transmission coefficient magnitude "V" shape behavior which induces a pulse compression in the time-domain.

2) L-LI TIME-DOMAIN RESPONSE

The L-li time domain analysis was performed in similar way as described in previous paragraph with a temporally

TABLE 4. Comparison NGD circuit performances.

Ref.	f_0 (GHz)	NGD (ns)	S_{21} (dB)	S_{11} (dB)	Length ×width size ($\lambda_g \times \lambda_g$)	Extra lumped components?
[26]	1.016	-2.09	-18.1	-33	0.41×0.41	*Y*
[31]	1.57	-8.75	-20.5	-32	0.39×0.19	*Y*
[32]	2.14	-1.03	-3.82	-12	-	*Y*
[33]	1	-1.5	-33	-25	0.78×0.06	*N*
[34]	1.97	-1	-2.2	-14	0.31×1.25	*N*
[35]	1.528	-2.89	-2.91	-11.9	0.41×0.32	*N*
This work	0.92	-3.72	-3.81	-11.4	0.58×0.08	*N*

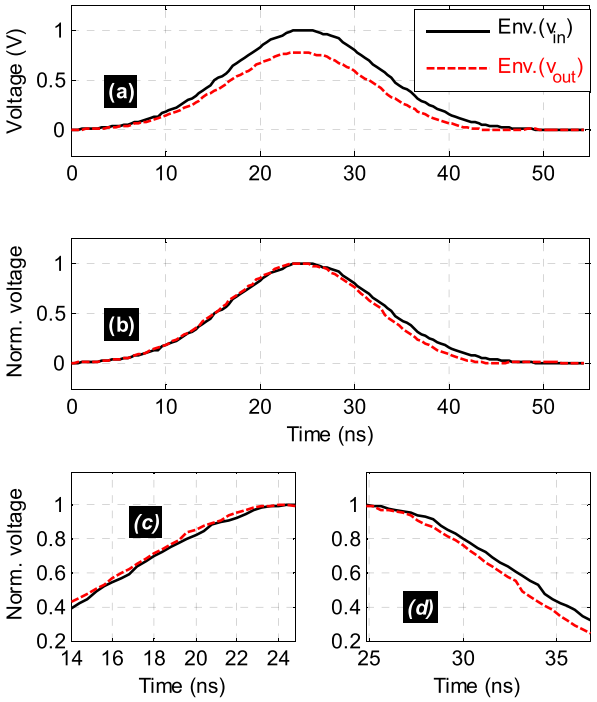

FIGURE 10. Input and output envelopes of S-li NGD circuit with (a) natural and (b) normalized, zooms in of (c) leading and (d) falling edges.

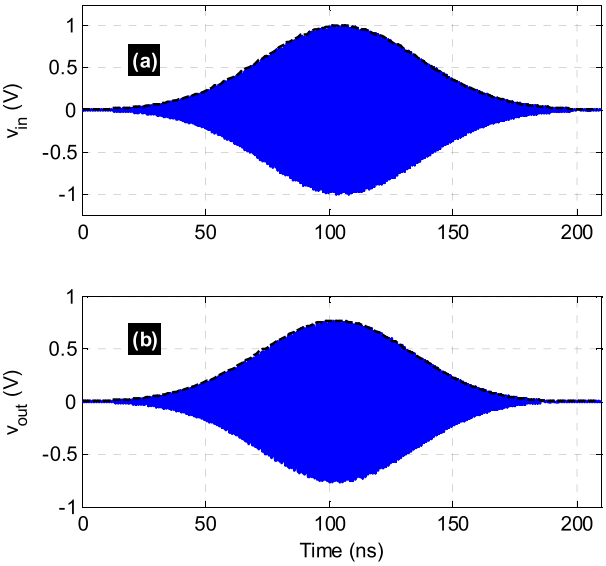

FIGURE 11. Input (in top) and output (in bottom) transient signals from L-li NGD circuit.

wider input signal modulating a since carrier with frequency $f_o = 0.92$ GHz. In this case, the Gaussian pulse presents a time width of about 200 ns as seen in Fig. 11(a). It was chosen in order to have a spectrum belonging in the NGD bandwidth of the L-li circuit shown in Fig. 8(a).

The transient plot of the L-li NGD circuit output is shown in Fig. 11(b). The associated envelopes are plotted in Fig. 12(a). It can be understood from the plot in Fig. 12(a) that the output signal is slightly attenuated compared to the input. In order to show the bandpass NGD significance, the normalized plots of the input and output envelopes are shown in bottom of Fig. 12(b). Two zooms in plots indicating the time advance of leading and trailing edges of the output compared to the input are indicated in Fig. 12(c) and in Fig. 12(d). In this case, the time-advance is more significant than the S-li previous results.

V. DISCUSSION ON NGD PERFORMANCES

In addition to the established theory and validation results, it would be necessary to situate the achievement of the presented li prototype compared to the published NGD circuits in the literature. Therefore, comparative study between the notable performances of the NGD li topology under investigation and the existing ones available in the literature [26], [31]–[35] are indicated here below in Table 4.

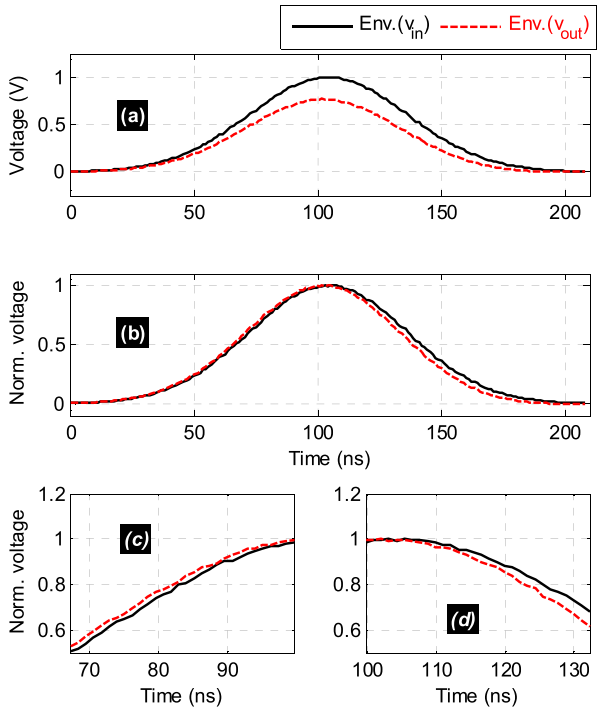

FIGURE 12. Input and output envelopes of L-li NGD circuit with (a) natural and (b) normalized, zooms in of (c) leading and (d) falling edges.

As matter of fact, it is noteworthy that the introduced li NGD topology presents the following advantages:

- Thanks to the li topology simplicity, the proposed NGD cell presents significant design flexibility compared to the circuits introduced in [9]–[11], [14]–[35],
- The li topology can be easily implemented with fully distributed elements without lossy lumped component,
- The li topology enables to realize an outstanding low signal attenuation better than 2.5 dB,
- And the access reflection losses can be matched easily without additional and external matching networks in the NGD bandwidth.

At this stage, non-specialist RF and microwave design engineers may wonder about the meaning and also the interpretation of li-topology bandpass NGD functions. Most of passive NGD investigations available in the literature did not answer to this curious misunderstanding. The possibility of bandpass NGD operation with this narrow NGD bandwidth in the time domain would be necessary. Doing this, to highlight more rigorously the bandpass NGD significance, transient analyses with modulated pulse signals will be examined in the next subsection.

VI. CONCLUSION

An innovative NGD topology of "li" geometrical shape is investigated. This outstandingly simple topology, never being studied before, is classified as a bandpass NGD function. The studied li NGD topology is comprised of only two parallel CL. This topology is a fully distributed circuit built with a lossy and delayed CL.

Deep li-NGD theory is developed from the S-matrix analytical modelling. The NGD analysis is established. The li NGD properties and characteristics are established. The mathematical expressions of NGD existence condition and NGD expressions at specific frequencies are discussed.

The li NGD theory is validated by designing and fabricating two prototypes in microstrip technology. Two prototypes of S- and L-li NGD microstrip circuits are designed and fabricated. It was shown by simulations and measurements that the li NGD circuits behave as bandpass NGD function. The simulated and measured GD and reflection, and transmission parameters are in very good agreement. More importantly, the possibility to propagate signal with envelope in time-advance is also investigated with both S- and L-li NGD prototypes. The time domain results are particularly innovative because the it was shown that the li-topology operates with time advance with remarkably low attenuated output.

Compared to the existing NGD circuits, the li NGD topology under study presents an advantage in terms of size reduction and flexibility to operate up to several GHz. Due to its potential integration, the developed NGD circuit is useful for the correction of the signal delays notably in the future RF and microwave devices and systems.

REFERENCES

[1] L. Brillouin, *Wave Propagation and Group Velocity*. New York, NY, USA: Academic, 1960.

[2] C. G. B. Garrett and D. E. McCumber, "Propagation of a Gaussian light pulse through an anomalous dispersion medium," *Phys. Rev. A, Gen. Phys.*, vol. 1, no. 2, pp. 305–313, Feb. 1970.

[3] S. Chu and S. Wong, "Linear pulse propagation in an absorbing medium," *Phys. Rev. Lett.*, vol. 48, no. 11, pp. 738–741, Mar. 1982.

[4] B. Segard and B. Macke, "Observation of negative velocity pulse propagation," *Phys. Lett. A*, vol. 109, no. 5, pp. 213–216, May 1985.

[5] L. Markley and G. V. Eleftheriades, "Quad-band negative-refractive-index transmission-line unit cell with reduced group delay," *Electron. Lett.*, vol. 46, no. 17, pp. 1206–1208, Aug. 2010

[6] J. N. Munday and W. M. Robertson, "Observation of negative group delays within a coaxial photonic crystal using an impulse response method," *Opt. Commun.*, vol. 273, no. 1, pp. 32–36, May 2007.

[7] S. Lucyszyn, I. D. Robertson, and A. H. Aghvami, "Negative group delay synthesiser," *Electron. Lett.*, vol. 29, no. 9, pp. 798–800, Apr. 1993.

[8] C. D. Broomfield and J. K. A. Everard, "Broadband negative group delay networks for compensation of microwave oscillators and filters," *Electron. Lett.*, vol. 36, no. 23, pp. 1931–1933, Nov. 2000.

[9] G. V. Eleftheriades, O. Siddiqui, and A. K. Iyer, "Transmission line models for negative refractive index media and associated implementations without excess resonators," *IEEE Microw. Wireless Compon. Lett.*, vol. 13, no. 2, pp. 51–53, Feb. 2003.

[10] O. F. Siddiqui, M. Mojahedi, and G. V. Eleftheriades, "Periodically loaded transmission line with effective negative refractive index and negative group velocity," *IEEE Trans. Antennas Propag.*, vol. 51, no. 10, pp. 2619–2625, Oct. 2003.

[11] O. F. Siddiqui, S. J. Erickson, G. V. Eleftheriades, and M. Mojahedi, "Time-domain measurement of negative group delay in negative-refractive-index transmission-line metamaterials," *IEEE Trans. Microw. Theory Techn.*, vol. 52, no. 5, pp. 1449–1454, May 2004.

[12] K.-P. Ahn, R. Ishikawa, A. Saitou, and K. Honjo, "Synthesis for negative group delay circuits using distributed and second-order RC circuit configurations," *IEICE Trans. Electron.*, vol. E92-C, no. 9, pp. 1176–1181, 2009.

[13] B. Ravelo, "Investigation on microwave negative group delay circuit," *Electromagnetics*, vol. 31, no. 8, pp. 537–549, Nov. 2011.

[14] S. Park, H.-J. Choi, and Y. Jeong, "Microwave group delay time adjuster," *IEEE Microw. Wireless Compon. Lett.*, vol. 17, no. 2, Feb. 2007, pp. 109–111.

[15] K.-J. Song, S.-G. Kim, H.-J. Choi, and Y.-C. Jeong, "Group delay time matched CMOS microwave frequency doubler," *J. Korean Inst. Electromagn. Eng. Sci.*, vol. 19, no. 7, pp. 771–777, Jul. 2008.

[16] K.-P. Ahn, R. Ishikawa, and K. Honjo, "Group delay equalized UWB InGaP/GaAs HBT MMIC amplifier using negative group delay circuits," *IEEE Trans. Microw. Theory Techn.*, vol. 57, no. 9, pp. 2139–2147, Sep. 2009.

[17] H. Choi, Y. Jeong, C. D. Kim, and J. S. Kenney, "Efficiency enhancement of feedforward amplifiers by employing a negative group-delay circuit," *IEEE Trans. Microw. Theory Techn.*, vol. 58, no. 5, pp. 1116–1125, May 2010.

[18] M. Kandic and G. E. Bridges, "Bilateral gain-compensated negative group delay circuit," *IEEE Microw. Wireless Compon. Lett.*, vol. 21, no. 6, pp. 308–310, Jun. 2011.

[19] B. Ravelo, "Distributed NGD active circuit for RF-microwave communication," *AEU-Int. J. Electron. Commun.*, vol. 68, no. 4, pp. 282–290, Apr. 2014.

[20] H. Mirzaei and G. V. Eleftheriades, "Realizing non-foster reactive elements using negative-group-delay networks," *IEEE Trans. Microw. Theory Techn.*, vol. 61, no. 12, pp. 4322–4332, Dec. 2013.

[21] T. Zhang, R. Xu, and C.-T.-M. Wu, "Unconditionally stable non-foster element using active transversal-filter-based negative group delay circuit," *IEEE Microw. Wireless Compon. Lett.*, vol. 27, no. 10, pp. 921–923, Oct. 2017.

[22] H. Mirzaei and G. V. Eleftheriades, "Arbitrary-angle squint-free beamforming in series-fed antenna arrays using non-foster elements synthesized by negative-group-delay networks," *IEEE Trans. Antennas Propag.*, vol. 63, no. 5, pp. 1997–2010, May 2015.

[23] L. He, W. Li, J. Hu, and Y. Xu, "A 24-GHz source-degenerated tunable delay shifter with negative group delay compensation," *IEEE Microw. Wireless Compon. Lett.*, vol. 28, no. 8, pp. 687–689, Aug. 2018.

[24] Y. Meng, Z. Wang, S. Fang, T. Shao, and H. Liu, "A broadband switchless bi-directional amplifier with negative-group-delay matching circuits," *Electronics*, vol. 7, no. 9, p. 158, Aug. 2018.

[25] M. Kandic and G. E. Bridges, "Asymptotic limits of negative group delay in active resonator-based distributed circuits," *IEEE Trans. Circuits Syst. I, Reg. Papers*, vol. 58, no. 8, pp. 1727–1735, Aug. 2011.
[26] Z. Wang, Y. Cao, T. Shao, S. Fang, and Y. Liu, "A negative group delay microwave circuit based on signal interference techniques," *IEEE Microw. Wireless Compon. Lett.*, vol. 28, no. 4, pp. 290–292, Apr. 2018.
[27] F. Wan, N. Li, B. Ravelo, Q. Ji, and J. Ge, "S-parameter model of three parallel interconnect lines generating negative group-delay effect," *IEEE Access*, vol. 6, pp. 57152–57159, 2018.
[28] G. Chaudhary and Y. Jeong, "Transmission-type negative group delay networks using coupled line doublet structure," *IET Microw., Antennas Propag.*, vol. 9, no. 8, pp. 748–754, Jun. 2015.
[29] B. Ravelo, "Theory of coupled line coupler-based negative group delay microwave circuit," *IEEE Trans. Microw. Theory Techn.*, vol. 64, no. 11, pp. 3604–3611, Nov. 2016.
[30] R. Das, Q. Zhang, and H. Liu, "Lossy coupling matrix synthesis approach for the realization of negative group delay response," *IEEE Access*, vol. 6, pp. 1916–1926, 2018.
[31] T. Shao, Z. Wang, S. Fang, H. Liu, and S. Fu, "A compact transmission-line self-matched negative group delay microwave circuit," *IEEE Access*, vol. 5, pp. 22836–22843, 2017.
[32] G. Chaudhary and Y. Jeong, "Negative group delay phenomenon analysis using finite unloaded quality factor resonators," *Prog. Electromagn. Res.*, vol. 156, pp. 55–62, Jun. 2016.
[33] C.-T.-M. Wu and T. Itoh, "Maximally flat negative group-delay circuit: A microwave transversal filter approach," *IEEE Trans. Microw. Theory Techn.*, vol. 62, no. 6, pp. 1330–1342, Jun. 2014.
[34] B. Ravelo, N. Li, F. Wan, and J. Feng, "Design, modeling and synthesis of negative group delay IL-shape topology," *IEEE Access*, vol. 7, pp. 153900–153909, 2019.
[35] F. Wan, N. Li, B. Ravelo, N. M. Murad, and W. Rahajandraibe, "NGD analysis of turtle-shape microstrip circuit," *IEEE Trans. Circuits Syst. II, Exp. Briefs*, to be published.

BLAISE RAVELO (Member, IEEE) is currently a University Full Professor with the Nanjing University of Information Science and Technology (NUIST), Nanjing, China. He is also a Lecturer on circuit and system theory, science, technology, engineering, and maths (STEM) and applied physics. He is a pioneer of the negative group delay (NGD) concept about t<0 signal travelling physical space. This extraordinary concept is potentially useful for anticipating and prediction all kind of information. He was research director of nine Ph.D. students (7 defended), postdocs, research engineers, and master internships. With USA, Chinese, Indian, European, and African partners, he is actively involved and contributes on several international research projects (ANR, FUI, FP7, INTERREG, H2020, Euripides^2, and Eurostars…). His research interest is on multiphysics and electronics engineering. He has been a member of the Scientific Technical Committee of the Advanced Electromagnetic Symposium (AES) since 2013. His Google scholar H-index in 2020 is 20. He is a member of research groups IEEE, URSI, GDR Ondes, Radio Society, and coauthored more than 250 scientific research articles in new technologies published in international conference and journals. He is member of *Electronics Letters* (IET) Editorial Board as a Circuit and System Subject Editor. He regularly invited to review articles submitted for publication to international journals (the IEEE Transactions on Microwave Theory and Techniques, the IEEE Transactions on Circuits and Systems, the IEEE Transactions on Electromagnetic Compatibility, the IEEE Transactions on Industrial Electronics, IEEE Access, IET CDS, IET MAP …) and books (Wiley, Intech Science…).

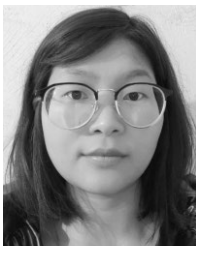

LILI WU received the B.Sc. degree in electrical engineering from Hefei Normal University, Hefei, China, in 2018. She is currently pursuing the M.S. degree with the Nanjing University of Information Science and Technology, Nanjing, China. Her research interests include negative group delay (NGD) and RF/microwave circuits.

FAYU WAN (Member, IEEE) received the Ph.D. degree in electronic engineering from the University of Rouen, Rouen, France, in 2011. From 2011 to 2013, he was a Postdoctoral Fellow with the Electromagnetic Compatibility Laboratory, Missouri University of Science and Technology, Rolla. He is currently a Full Professor with the Nanjing University of Information Science and Technology, Nanjing, China. His current research interests include negative group delay circuits, electrostatic discharge, electromagnetic compatibility, and advanced RF measurement.

WENCESLAS RAHAJANDRAIBE (Member, IEEE) received the B.Sc. degree in electrical engineering from Nice Sophia-Antipolis University, France, in 1996, the M.Sc. degree (Hons.) in electrical engineering from the Science Department, University of Montpellier, France, in 1998, and the Ph.D. degree in microelectronics from the University of Montpellier. Since 1998, he has been with the Informatics, Robotics and Microelectronics Laboratory of Montpellier (LIRMM), Microelectronics Department. Since 2003, he has been with the Materials, Microelectronics and Nanoscience Laboratory of Provence (IM2NP), Microelectronic Department, Marseille, France, where he was an Associate Professor. Since 2014, he has been a Professor with Aix Marseille University, where he heads the Integrated Circuit Design Group, IM2NP Laboratory. He is currently a Full Professor with the University of Aix-Marseille. His research is focused on the design of analog and RF IC's for telecommunication systems and for smart sensor ultralow power IC interfaces. He has served on program committees of IEEE NEWCAS and ICECS. He has been and is a Reviewer of contributions submitted to several IEEE conferences and journals such as ISACS, NEWCAS, MWSCAS, ESSCIRC, ESSDERC, RFIC, and the IEEE Transactions on Circuits and Systems I and II.

NOUR MOHAMMAD MURAD (Member, IEEE) was born in Saint Denis of La Réunion, France, in 1974. He received the Ph.D. degree in communication and electronics from the Ecole Nationale Supérieure des Télécommunications (Telecom Paris), in 2001. From 1998 to 2001, he served as an Engineer R&D with Alcatel CIT. During this period, he prepared the Ph.D. thesis with Télécom Paris in parallel. From 2001 to 2003, he worked as a Teacher and a Researcher with the University of La Reunion, where he had co-responsibility on the coupling between energy and telecommunication project. From 2004 to 2007, he was an Assistant Professor Researcher with the 3IL Engineering School and a Researcher with XLIM/OSA, Limoges University. Since September 2007, he has been an Assistant Professor Researcher with the University of Reunion. In 2018, he obtained his Accreditation to Direct Research (HdR) in numerical communications and networks. He became an Associate Professor in 2019 and was responsible of a team research on "Energy Optimization for Sensor Networks" (5 researchers). He directed and co-supervised five Ph.D. and four master's students. He was the scientific co-responsible of projects titled ORIANA ANR and FEDER CARERC. Its research relates to the numerical communication and RF, signal, and information theory with a specific accent on wireless communications, spread spectral techniques, synchronization, MIMO systems, techniques diversity, wireless energy transportation, antenna networks, and wireless sensor networks.